Research Article

Touqeer Ahmad[#], Fazal Mabood[#], Rizwana Sarwar[#], Ajmal Khan*, Sobia Ahsan Halim, Najeeb Ur Rehman, Rene Csuk, Ricard Boque, and Ahmed Al-Harrasi*

A highly sensitive β-AKBA-Ag-based fluorescent "turn off" chemosensor for rapid detection of abamectin in tomatoes

https://doi.org/10.1515/gps-2023-0239
received November 21, 2023; accepted June 04, 2024

Abstract: This study presents the synthesis of a sensitive AKBA-Based fluorescent "Turn off" chemosensor for rapid detection of abamectin residues in tomatoes. Silver nanoparticles were synthesized by using 3-*O*-acetyl-11-keto-β-boswellic acid (β-AKBA) by chemical reduction method. The characterization of AKBA-AgNPs was performed by UV–vis spectroscopy, Fourier transform infrared spectroscopy (FTIR), and transmission electron microscopy (TEM). The average particle size of NPs was found to be 46.2 ± 2 nm with lumps of macro-sized particles. TEM data further revealed that nanoparticles were polydispersed and spherical in shape and also show good stability at high temperatures and pH. The biosensing properties of nanoparticles were studied for the detection of abamectin residues in tomato samples. Abamectin a natural product derived from the bacterium *Streptomyces avermitilis* is effective against a wide range of pests. In sensing protocol 67 organic tomato samples were segregated into 34 (safe group, without a spray of abamectin) and 33 samples (as an unsafe group, sprayed with abamectin insecticide solution). Emission spectra of these sample solutions were measured in the wavelength range of 450–530 nm, excitation wavelength was fixed at 488 nm. The effect of minor wavelength variation for the discrimination and classification of the two groups was investigated by applying two chemometric methods including partial least square discriminant analysis and principal component analysis with projection. The mechanism of its interaction between the AKBA-Ag NPs and abamectin residue was also established through UV/visible, FTIR, and TEM microscopy. This newly synthesized nanoparticle was found to have excellent stability at variables, i.e., temperature, storage period, salt concentration, and pH. Therefore, the synthesized Ag NPs are potential candidates for biosensing applications against abamectin.

Keywords: β-AKBA, frankincense, silver nanoparticles, chemosensor, abamectin, insecticide, emission spectroscopy, PLS-DA, PCA projection, tomatoes

1 Introduction

The increasing global population leads to, severe concerns for agriculture, food storage, and processing and constitutes big challenges to food safety. Use of pesticides in agriculture leads to food contamination, which results in severe health issues [1]. Various analytical methods such as HPLC (high-performance liquid chromatography), MS (mass spectrometry), and GC (gas chromatography) have been employed for the detection of pesticides in food but they are time-consuming, economically non-effective, and required skilled persons [2]. In addition, several enzymatic methods and immunoassay tests were performed to detect pesticides using optical and electrochemical study methods. Enzymatic methods exhibit good sensitivity but have fraught

# Equal contributions.

* **Corresponding author: Ajmal Khan**, Natural and Medical Sciences Research Center, University of Nizwa, P.O. Box 33, Birkat Al Mauz, Nizwa, 616, Sultanate of Oman, e-mail: ajmalkhan@unizwa.edu.om, tel: +968254463502
* **Corresponding author: Ahmed Al-Harrasi**, Natural and Medical Sciences Research Center, University of Nizwa, P.O. Box 33, Birkat Al Mauz, Nizwa, 616, Sultanate of Oman, e-mail: aharrasi@unizwa.edu.om, tel: +96825446328
Touqeer Ahmad, **Sobia Ahsan Halim**, **Najeeb Ur Rehman:** Natural and Medical Sciences Research Center, University of Nizwa, P.O. Box 33, Birkat Al Mauz, Nizwa, 616, Sultanate of Oman
Fazal Mabood: Institute of Chemical Sciences, University of Swat, Swat, Pakistan
Rizwana Sarwar: Department of Chemistry, COMSATS University Islamabad, Abbottabad Campus, Abbottabad, 22060, KPK, Pakistan
Rene Csuk: Organic Chemistry, Martin-Luther University Halle-Wittenberg, Kurt-Mothes-Str. 2, D-06120, Halle (Saale), Germany
Ricard Boque: Department of Analytical Chemistry and Organic Chemistry, Universitat Rovira i Virgili, Tarragona, Spain

due to poor enzymatic/antibody stability that restricts its wide use [3,4]. With the advancement of the nanotechnology arena, nanomaterial-based biosensors have attracted considerable attention due to their high sensitivity and low cost. Metal nanomaterials [5], semiconductor quantum dots [6], and carbon nanomaterials [7] have been employed in design and fabrication of ultrahigh sensitive biosensors with novel surface plasmon resonance (SPR), fluorescence behavior, and electrochemical properties. U.S. Environmental Protection Agency highlighted in 2011, the total amount of pesticides used in 2007 United States was 1.1 billion pounds [8]. European water policy enlists pesticides as a priority hazardous and their harmful impact on the environment [9]. To avoid adverse health, pesticide residue levels (MRL) in food have been studied regularly by employing biosensor technology [10–12]. Biosensors provide a new insight into maintaining food quality using sophisticated and tailored analytical tools with specificity, reliability, and low cost over short intervals of time [13]. Manipulating nanomaterial size and shape results in novel sensing devices with enhanced biosensor performance and reproducibility [14].

Several types of nanomaterials such as nanocomposites, nanofibers, nanoflowers, semiconductor quantum dots and carbon quantum dots, and carbon nanotubes (CNTS) have been employed for biosensor development because of their novel physical, chemical, mechanical, magnetic, optical properties and high electrical conductivity [15–18]. Abamectin, a macrocyclic lactone [19], and fermentation product of avermectins, which are naturally derived from the soil bacterium *Streptomyces avermitilis.* According to literature Abamectin, showed nematicidal, acaricidal, and insecticidal activity [20]. Major current applications of abamectin involve the uses of citrus, ornamental plants, pears, cotton, and vegetable crops in the range of 5–27 g abamectin per hectare as a foliar spray [21]. Abamectin is widely used in veterinary and agriculture, against a variety of animal parasites and insects, can drain off from the sites of application, and becomes environmentally hazardous. The compound and its metabolites have adverse effects on living organisms due to its high toxicity even at very low concentrations [22]. Because of its broad-spectrum antiparasitic efficacy against both internal and external paras, Abamectin residues can occur in a variety of food products (e.g., fruits, vegetables, fish, meat, eggs, and milk), and they can also accumulate in the environment by spraying, drifting, when it is used excessively or unnecessarily [23]. Residues of abamectin in food and the environment pose a threat to human health and can result in disorders affecting the neurological, endocrine, reproductive, and digestive systems [24]. The investigation of abamectin residue in food products and its potential risk have gained the attention of researchers, and the maximum residue limits (MRLs) of abamectin have been established by Codex Alimentarius Commission and the European Union.

The MRLs of abamectin in animal-derived food products range from 10 to 100 $\mu g \cdot kg^{-1}$, while in fruits and vegetables, they range from 5 to 20 $\mu g \cdot kg^{-1}$ [24]. Fruits and tomatoes have maximum residue levels (MRLs) of 0.01 to 0.02 $mg \cdot kg^{-1}$ defined by the Codex Committee on Pesticide Residues under the Joint FAO/WHO Food Standards Program [25]. In order to protect human health and food safety, it is now important to determine the presence of trace abamectin residue in food samples. Many fluorescent pesticide sensors based on nanomaterials employ nanoparticles, which are spherical particles with nanoscale dimensions. The abamectin detection in terms of sensing agent/molecule, mechanism, Ag NP size, linear detection range, LOD, and applicability to different samples is given in Table 1.

To ensure food safety, biosensors that use nanoparticles provide a simple, low-cost, and reliable method of detecting pesticides in food matrices. For precise pesticide

Table 1: The abamectin detection by different materials

Material type	Detection mechanism	Size range	Linear detection range	LOD	Ref
Gold nanoparticles (AuNPs)	Colorimetric	10–100 nm	$ng \cdot mL^{-1}$–$\mu g \cdot mL^{-1}$	$ng \cdot mL^{-1}$	[26]
Quantum dots (QDs)	Fluorescence	N/A	0.05 to 10.0 $\mu g \cdot L^{-1}$	0.05 $\mu g \cdot L^{-1}$	[27]
Magnetic nanoparticles	Magnetism	95–195 nm	0.9–1,000 $\mu g \cdot L^{-1}$	0.2 $\mu g \cdot L^{-1}$	[28]
Magnetic Fe_3O_4 microspheres	Magnetism	—	2–5,000 $\mu g \cdot L^{-1}$	0.18 $\mu g \cdot L^{-1}$	[29]
Mesoporous alumina	LC-MS/MS	N/A	0.02–0.50 $mg \cdot L^{-1}$	0.16 $ng \cdot g^{-1}$	[5]
Antibody	Immunoassay	N/A	$pg \cdot mL^{-1}$–$ng \cdot mL^{-1}$	1.07 $ng \cdot mL^{-1}$	[30]
Carrez's reagent	On-line SPE	N/A	0–15 $ng \cdot mL^{-1}$	0.67 $ng \cdot mL^{-1}$	[31]
Aptamer	Aptamer-based assay	N/A	$ng \cdot mL^{-1}$–$\mu g \cdot mL^{-1}$	$ng \cdot mL^{-1}$	
Molecularly imprinted polymer (MIP)	Molecular imprinting	N/A	0.03–1.50 $\mu g \cdot mL^{-1}$	0.02 $ng \cdot mL^{-1}$	[32]
Fluorescent probe	Fluorescence detection	N/A	1.3 $\mu g \cdot L^{-1}$	4.41 $\mu g \cdot L^{-1}$	[33]
Fe_3O_4@TzDa	HPLC-FLD	~200 nm	0.05–500 $\mu g \cdot L^{-1}$	0.015 $\mu g \cdot L^{-1}$	[34]

detection, these nanomaterial-based biosensors take advantage of the increased sensitivity and selectivity that nanomaterials offer. Pesticides and other small compounds have been detected by using metallic nanoparticles such as silver, gold, titanium, and other materials (such as TiO_2^- and CdS-decorated graphene nanocomposite).

Therefore, rapid, and sensitive detection of abamectin is important for health and environmental preservation. Reports on the environmental fate of abamectin and its adverse effects on living organisms are well known [22]. 3-*O*-Acetyl-11-keto-β-boswellic acid (one of the most active triterpenoids) was isolated from various species of the genus *Boswellia* [35,36] together with other biologically active triterpenes [37]. The AKBA has many pharmacological activities, such as anti-inflammatory, antioxidant [38], anti-tumor [39], and anti-aging [40]. AKBA was effective for bacterial infection [41] and has also been found to be effective against the SARS-CoV-2 virus through its ability to bind functional proteins of the virus [42]. The aim of the current study is to develop AKBA-loaded Ag nanoparticle biosensors for the detection of abamectin in vegetables and water at minimum low concentrations

2 Materials and methods

2.1 Materials

Silver nitrate ($AgNO_3$) and methanol MeOH were purchased from Sigma-Aldrich (MO, USA). Sodium hydroxide (NaOH), hydrochloric acid (HCl), and sodium hydroxide ($NaBH_4$) were procured from Merck (NJ, USA). The pH of nanoparticles was adjusted by Thermo Electron Corporation (MA, USA) pH meter by using an IM solution of HCl and NaOH. The chemicals used in the current study were of analytical grades. Ambactin (CAS: 71751-41-2) was purchased from the agriculture department.

2.2 Sample collection, and purification

Boswellia sacra gum resin is collected from various locations in Dhofar, Oman (2012) and authenticated by the plant taxonomist at the herbarium of the Natural and Medicinal Sciences Research Center (NMRSC), University of Nizwa, Oman. A voucher specimen (BSHR-01/2012) was deposited at the NMRSC Center.

The air-dried material (1 kg) of *B. sacra* resin was exhaustively extracted with distilled methanol for three days. The rotary evaporator was used to remove solvent to yield concentrated methanolic extract *800 g.

For isolation of AKBA, MeOH extract was loaded on silica gel column chromatography (CC); (70–230 mesh; Merck) and eluted with increasing polarity of *n*-hexane/ethyl acetate up to 100% EtOAc. A total of twelve fractions, BS_1–BS_{12} were obtained through column chromatography. The fraction BS_4 (350 mg) obtained with 30% EtOAc/*n*-hexane was selected and further injected on preparative chloroform (fermented with 0.6% Ethanol) HPLC to get AKBA (210 mg) as a UV-active compound at a retention time of 42 min with 3 mL·min^{-1} flow rate.

2.3 Synthesis, stability, and reaction optimization of nanoparticles

AKBA-conjugated silver nanoparticles were synthesized by slight modification in our previous study [43]. The ratio of silver nitrate to AKBA was adjusted 1:1 ($AgNO_3$: AKBA) as shown in Figure 1.

The reaction mixture ($AgNO_3$: AKBA) was set on a magnetic hot plate with temperature and rotation settings at 100°C and 400 rpm. After 5 min, add a few drops of sodium borohydride (3 mM) and let the mixture for complete reduction for one hour. The UV–VIS was performed to confirm the synthesis after the visual color change of the mixture. The synthesized nanoparticles were centrifuged at 15,000 rpm for 20 min. The supernatant was removed leaving behind a pellet containing aggregate. The pellet was first washed with methanol and then with double distilled water to remove extra reducing agents and ions.

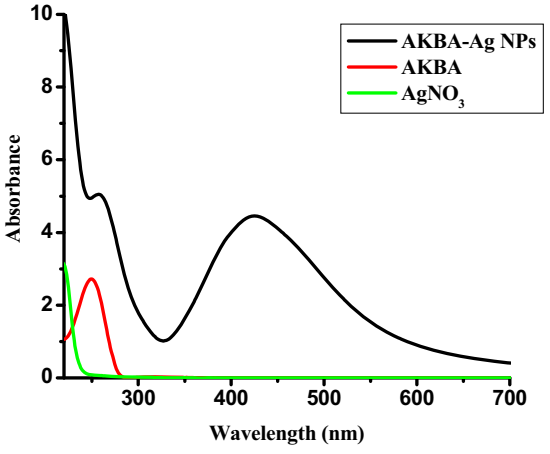

Figure 1: Synthesis of AKBA-Ag NPs.

2.4 Stability of synthesized nanoparticles

The stability potential of AKBA-Ag NPs was tested against different pH (3–13), temperature, and brine solutions. The UV–Vis spectra were recorded to confirm the stability of nanoparticles. The pH of nanoparticles was checked from Digital pH metre model 510 (Oakton, Eutech). IM solution of HCl and NaOH was prepared in distilled water. The synthesized nanoparticles were heated in a round bottom flask for 30 min at 25, 50, 75 and 100°C. The UV spectra of the solution were then recorded to confirm the stability. A brine test was performed.

2.5 Fourier transform infrared spectroscopy (FTIR)

FTIR analysis of nanoparticles is an important spectroscopic technique used to characterize the chemical composition, functional groups, and surface properties of synthesized material. FTIR spectra for AKBA and AKBA-Ag NPs were recorded on an IR spectrophotometer (IR-460 Shimadzu, Kyoto, Japan). The mode of interaction between AKBA-Ag NPs and abamectin was also studied via FTIR analyses.

2.6 Transmission electron microscope (TEM)

TEM is used to determine the nanoparticle size, shape, and morphology by using TEM (Model: JEOL, TEM-1400 Electron Microscope), operated at an accelerating voltage of 110 kV. The nanoparticles were deposited onto a carbon-coated copper TEM grid. To ensure accurate imaging, the sample must be thinly sectioned or dispersed to form a monolayer of nanoparticles.

2.7 Stability at physiological pH of tomato

Optimization of the pH is significant for biosensor applications due to its role in complex formation and deformation [44]. Therefore, AKBA-Ag NPs pH stability is important for sensing protocol. No significant change in SPR band was observed in basic and acidic medium.

2.8 Sensing protocols

Biosensing potential of AKBA-Ag NPs was investigated against different available pesticides (Abamectin, Revus Top, Alpha-Sumi, Ex-Advance, and Revus). Pesticide solutions (100 µM) were mixed with AKBA-Ag NPs in a 1:1 (v/v) ratio for ~20 min at RT (~30 ± 3°C). The primary interactions of Abamectin and AKBA-Ag NPs were confirmed by UV–Vis spectroscopy and further confirmed by fluorescence spectroscopy. The mechanism of aggregation or interaction mechanism was established in time-dependent manner after interacting with an equal volume of AKBA-Ag NPs and pesticides (i.e., Abamectin). The sensing selectivity of AKBA-Ag NPs towards pesticide (e.g., Abamectin) was further evaluated by mixing a fixed concentration of AKBA-Ag NPs (1 mL) with sensed pesticide (1 mL) and other interfering pesticides (1 mL) by UV–vis spectroscopy. The effect of pH (3–13) on AKBA-Ag NPs was also studied to check the binding efficiency in the actual medium. AKBA nanoparticles were found stable against different ranges of pH, so they possess sensing capability at all ranges of pH.

2.9 Application in real sample of tomato

Around 67 organic tomato samples were purchased from Grand Mall and LuLu Hypermarkets, Nizwa, Oman, washed with distilled water, and stored at 5°C until further use. Thirty-four tomatoes without treatment were used as an abamectin residue-free set (safe group). On the other hand, 33 tomato samples (unsafe group) were sprayed with abamectin (avermectin b1) insecticide solution prepared by diluting 1 mL of insecticide solution (10 ng·µl^{-1}) in 500 mL of distilled water. After storing all the samples for 1 day at 5°C, next day each tomato sample was ground, filtered, and washed with distilled water.

To each filtrate, 1 mL of AKBA nanoparticle solution was added and marked up to 100 mL with water. The abamectin insecticide sensing ability for the newly synthesized chemosensor (AKBA-Ag NPs) was monitored by using a Fluorescence Spectrofluorophotometer (RF-5301PC, Shimadzu, Japan). Emission spectra of all solutions were measured in the wavelength range of 450–530 nm, excitation wavelength was fixed at 488 nm, and slit width for both excitation and emission was kept at 20 nm under low intensity using Hellma fluorescence cuvettes made of quartz of 0.1-mm optical path length.

2.10 Data analysis

All data analyses were performed through Unscrambler software X10.3 (CAMO Software, Oslo, Norway) and Microsoft Excel 2016 software.

3 Results and discussion

3.1 Synthesis, stability and reaction optimization of nanoparticles

Reaction conditions such as pH, temperature, concentration, mixing speed, and exposure time need to be optimized to run a precise and up-scalable process for the synthesis of stable nanoparticles. Nanoparticle synthesis took place rapidly with the addition of a reducing agent from the conversion of Ag^{+1} to Ag^{0} by constant stirring. After color change, synthesis was confirmed by UV–Vis spectroscopy. The strong absorption peak at 412 nm confirmed the nanoparticle synthesis.

3.2 Reaction optimization at different pH

The reaction optimization and stability potential of AKBA-Ag NPs were tested against different pH (3–13) for optimization. The pH of nanoparticles was adjusted by Thermo Electron Corporation (MA, USA) pH meter by using an IM solution of HCl and NaOH. The UV–visible spectra were recorded after 4 h of pH adjustment. The UV–Vis data support the stability of AKBA-Ag NPs on all pH. The peak at pH 2–3 showed a decrease in absorption intensity with peak broadening (Figure S1). The increase in the intensity of the SPR peaks was observed by increasing pH. A red shift was observed when the medium was changed from acidic to neutral (pH, 7–8). Moreover, AgNPs' SPR peak λ_{max} values have almost been constant. It clearly explained that the pH 7 reaction mixture is most suitable for reducing Ag+ ions into AgNPs and is stable over a month.

AKBA conjugated silver nanoparticles were found less stable in extremely basic conditions as compared to neutral pH (Figure S1). The synthesized silver nanoparticles were less stable in an acidic medium because the availability of proton decreases the interaction between the capping agent and nanoparticles surface and nanoparticles aggregate were formed [45]. Based on the observed UV–Vis peaks' variation and persistence, the stability of the nanoparticles was ascertained.

3.3 Temperature effect

Reaction optimization and Stability of AKBA-Ag NPs were studied at different ranges of temperatures. The temperature reaction conditions were checked by heating the nanoparticle solution at four different temperature ranges (25, 50, 75, and 100°C) for 30 min. The effect of temperature on λ_{max} and SPR was observed using UV–Vis spectrophotometer. An increase in reaction rate was observed with increasing temperature. The higher the temperature, the faster the reduction from Ag^{+1} to Ag^{0} (Figure S2). Based on the observed UV–Vis peaks' variation and persistence, the stability of the nanoparticles was ascertained. After pH and temperature optimization, the reaction conditions for nanoparticle synthesis were adjusted at pH 7 and 100°C. So the temperature of 100°C is considered as the optimum condition for nanoparticle synthesis [46].

3.4 FTIR analysis

FTIR analyses of AKBA and AKBA-Ag NPs were recorded to check the main functional group responsible for the syntheses of NPs. The eminent peaks in the drug FTIR spectrum were found at 1,243, 1,735, 2,921, and 2,360 cm^{-1}. After the drug's reaction with $AgNO_3$, the peak at 1,243 cm^{-1} was shifted to a higher wave number side 1,305 cm^{-1} which was due to the C–O stretching vibration of ketone moiety [47]. The intense band noticed in the drug at 1,735 cm^{-1} confirmed the presence of the carboxylic acid (C═O stretching vibration) group. Another distinguished peak at 2,921 cm^{-1} was ascribed to C–H stretching vibration [47]. This band disappeared in the case of nanoparticles FTIR Spectra (as shown in Figure 2). The immediate decline and capping of Ag ion into Ag nanoparticles in the current analysis might be due to the carboxylic group (disappeared in the case of silver nanoparticles) (Figure 2).

It was recorded to check the main functional group responsible for syntheses of NPs. The eminent peaks in the AKBA FTIR spectrum were found at 1243, 1735, 2921, and 2,360 cm^{-1}. After AKBA reaction with $AgNO_3$, the peak at 1,243 cm^{-1} was shifted to a higher wave number side 1,305 cm^{-1} which was due to the C–O stretching vibration of ketone moiety [47]. The intense band noticed in the drug at 1,735 cm^{-1} confirms the presence of the carboxylic acid (C═O stretching vibration) group. Another distinguished peak at 2,921 cm^{-1} was ascribed to C–H stretching vibration [47]. This band disappeared in the case of nanoparticles FTIR Spectra (as shown in Figure 2). The immediate decline and capping of Ag ion into Ag nanoparticles in the current analysis might be due to the carboxylic group (disappeared in the case of silver nanoparticles; Figure 2).

The mode of interaction between AKBA-Ag NPs and abamectin was studied via FTIR analyses. The prominent peaks in FTIR spectra of abamectin were found at 3,400 cm^{-1}

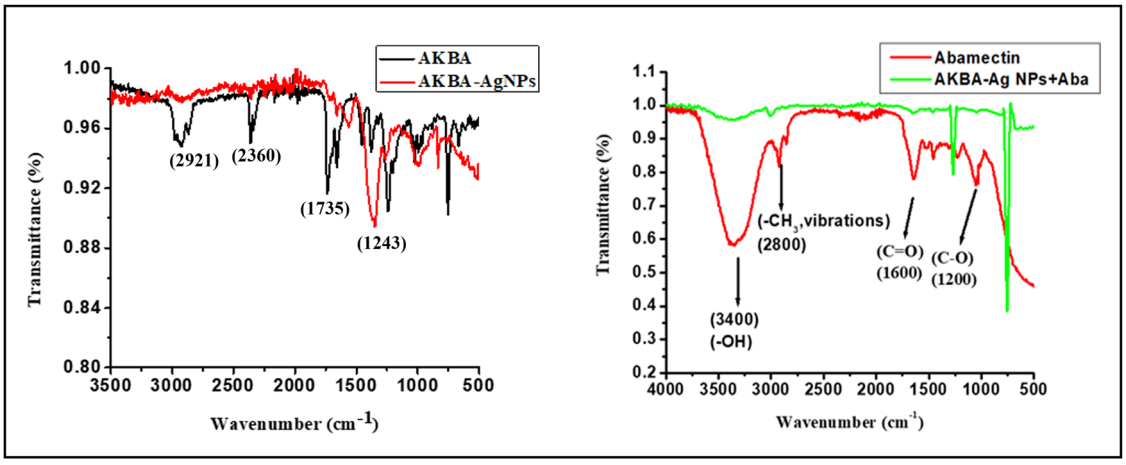

Figure 2: FTIR spectral analysis of AKBA, AKBA-Ag NPs, and AKBA-Ag NPs plus abamectin.

(–OH stretching vibrations of alcohol) 2,900 cm^{-1} ($–CH_3$ stretching), 1,600 cm^{-1} (–C═O stretching vibration), 1,200, and 1,100 cm^{-1} is characteristic of bending vibrations of –C–OH and $–OCH_3$ respectively. When abamectin complexes with AKBA-Ag NPs, the band assigned to –OH group diminished greatly. Moreover, peaks related to the –C═O and $–OCH_3$ functional group show a blue shift in spectra. Bands in the physical mixture are a combination of AKBA-Ag NPs and abamectin complex, whose FTIR spectra were much different from abamectin. FTIR spectral analyses show the interaction of –OH of abamectin with AKBA-A NPs surface, which results in cross-linking of two molecules. Polar groups like –C═O, $–OCH_3$ result in non-electrostatic interaction with nano surface (Figures 2 and 12). Our results are in close agreement with the data published in literature [48].

3.5 TEM analyses

Bright-field images of AKBA-Ag NPs were recorded for particle size and shape determination using TEM. TEM data revealed that nanoparticles were polydispersed and spherical in shape. Synthesized nanoparticles possess symmetry in their shape and are of variable size. Average particle size of NPs was found to be 46.2 ± 2 nm with lumps of macro-sized particles (Figure 3).

3.6 Pesticides chemo-sensing

AKBA-Ag NPs biosensing potential was checked against various pesticides such as Abamectin, Revus Top, Alpha-Sumi, Ex-Advance, and Revus in water. Different concentrations (10–100 ppm) of fresh pesticide solutions were prepared and their fluorescence spectra with and without nanoparticles were recorded. AKBA-Ag NPs displayed an excellent potential for detection of Abamectin in water.

3.7 Chemosensing and emission spectra interpretation

Figure 4 show the representative emission spectra of both the safe and unsafe groups of tomato samples in the ranges of 450–530 nm.

The emission spectra of the tomato samples in the safe and unsafe groups almost overlapped. The emission wavelengths of the emission spectra of the tomato samples from the safe and unsafe groups differ slightly. The emission peak for the safe group is located at 490.4 nm, and for the unsafe group, it is located at 489.4 nm The difference between the emission spectra of the two groups is only one nm. The chemometric techniques principal component analysis (PCA) and partial least square discriminant analysis (PLS-DA) were applied to emission spectra in order to determine the impact of this slight wavelength fluctuation.

3.8 Partial least squares-discriminant analysis (PLS-DA)

PLS-DA was accomplished for classification and discrimination of two groups of tomato samples labeled as safe group (no-spray of insecticide solution) and unsafe group (tomato samples sprayed with abamectin solution). PLS-DA models were built using the Kernel-NIPALS algorithm with an iteration value of 100. In short, PLS-DA is a controlled procedure based primarily on modeling variability between

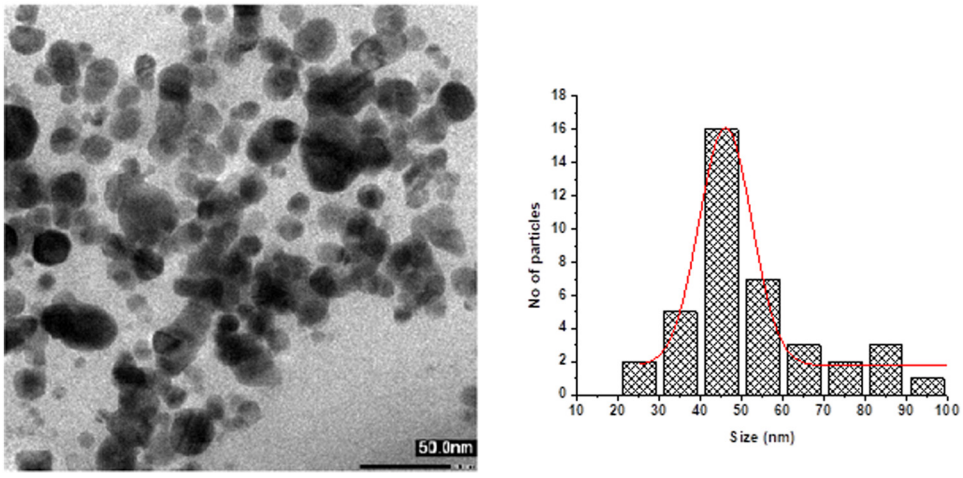

Figure 3: TEM Images of AKBA-Ag NPs and particle size distribution.

different classes by using the PLS calibration model to distinguish unknown samples. In the current study, the PLS model transmitted the spectral alterations (*X*) to the consigned dummy variables (*Y*) by maximizing the covariance between them. As there are only two assigned classes to differentiate, therefore, this ideal model used one category as a response variable (*Y*) coded for each class as follows: membership of one class was assigned −1, while membership for another class was designated as +1. Each unidentified analyte was taken as a forecast value (between −1 and +1) after predicting with the established PLS model. An analyte with a predicted value adjacent to −1 was allocated to one class, while a sample with the expected value close to +1 was identified as the other class. However, a value adjacent to zero indicated that the sample did not belong to any of the classes, specifically when the projected deviation or uncertainty of the predicted value is zero.

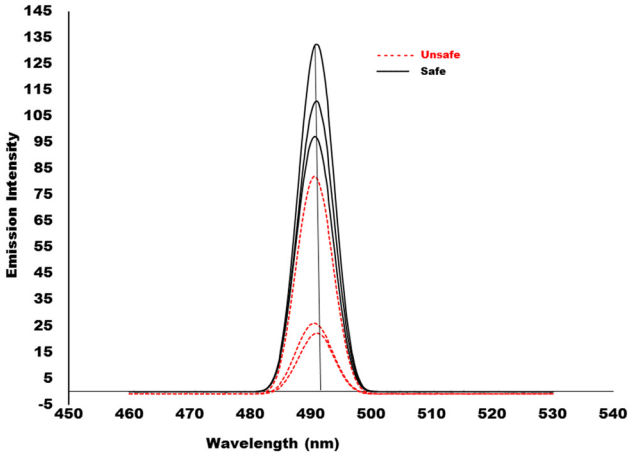

Figure 4: Representative emission spectra (not pre-processed) of both the safe and unsafe group tomato samples.

The raw emission spectra were split into two sets, i.e., a training test including 70% of all the spectral data to build the PLS-DA calibration model and a test set with 30% of spectral data to externally validate the PLS-DA calibration model. The tested samples from the training set were randomly chosen. The same model (PLS-DA calibration) was also internally validated, consuming a full cross-validation method and investigating the maximum of 7 latent variables (LVs). Before PLS-DA modeling, unit vector normalization, multiplicative scatter correction (MSC) and standard normal variate (SNV), smoothing, first (D1) and second (D2) derivatives of the spectra built on the bases of Savitzky–Golay algorithm having 5 smoothing points and 2 polynomial order, were also tried. However, all those spectral transformations did not improve the PLS-DA models. The accuracy, precision, and optimization of the developed PLS-DA models were assessed based on having the lowest values of root mean square error cross-validation (RMSECV), co-efficient of determination (R^2), number of factors and root mean square error of prediction (RMSECV), and the highest percentage of correctly classified samples concerning calibration and external validation sets. The results of various types of spectral transformation for PLS-DA models are given in Table 2.

Results in Table 2 indicated that PLS-DA models for not-processed emission spectra give the best ability to classify the unidentified samples. The total percentages of correctly classified samples for not-processed emission spectra for both the calibration and prediction sets were found 100%. It perfectly discriminated the samples into two groups (safe and unsafe) based on the presence of abamectin residue. In the calibration set, there were 34 samples of the safe group and all of those were 100% classified as safe (not sprayed with abamectin solution). Similarly, samples of the unsafe group in the calibration set were 33

Table 2: Results of PLS-DA models for discrimination of safe and unsafe tomato samples based on the presence of abamectin insecticide

Pre-processing	Calibration set correctly classified (%)					R^2	Prediction set correctly classified (%)				R^2
	LVs	Total	Pure (safe) tomato samples	Sprayed (unsafe) tomato samples	RMSECV		Total	Pure (safe)	Sprayed (unsafe)	RMSEP	
Nil pre-processing	2	67	34 − 0 = 34	33 − 0 = 33	0.066	0.995	27	15 − 0 = 15	12 − 0 = 12	0.069	0.995
Smoothin 1 with 7	2	67	34	33	0.065	0.995	27	15	15	0.071	0.994
Unit vector normalization	1		33 − 0 = 33	36 − 5 = 31	0.579	0.669	30	15	14	0.591	0.650
MSC	1		2	5	0.995	0.027	30	0	3	0.981	0.036
MSC + unit vector normalization	2		0	4	0.999	0.023		1	3	0.966	0.065
SNV	1		1	4	1.024	0.004		1	2	0.971	0.055
SNV + unit vector normalization	2		2	3	0.999	0.022		2	3	0.973	0.525
D1	5		0	0	1.23	0		0	0	1.21	0
D2	5		0	0	1.220	0		0	0	1.200	0
MSC + D1	5		2	4	1.013	0.019		0	0	0	0

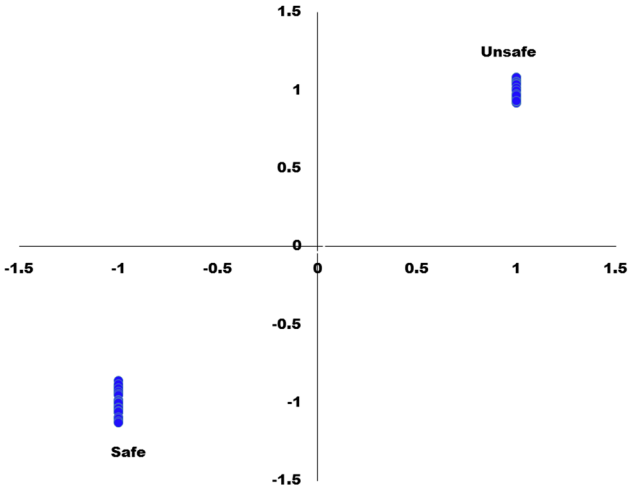

Figure 5: Predicted versus reference values plot for calibration model of safe and unsafe tomato samples based on the presence of abamectin insecticide.

samples and were 100% classified too. The result indicated that PLS-DA models for not-processed emission spectra are the optimum ones, based on a compromise the lowest values of RMSECV = 0.066 and R^2 = 0.995 for calibration set, the lowest values of RMSEP = 0.069 and R^2 = 0.995 for the prediction set, the least number of factors, i.e., 2 and 100% classification among the samples of safe and unsafe tomatoes for both the calibration and prediction sets.

The predicted versus reference values for this optimum calibration model are presented in Figure 5.

This plot in Figure 5 displayed how close to the ideal values of −1 and +1 of both safe and unsafe groups. The score plots for factor 1 and factor 2 of the PLS-DA model are also described in Figure 6.

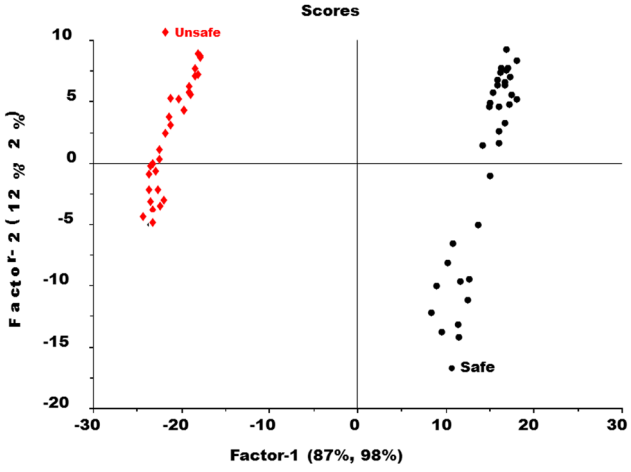

Figure 6: Score plot of PLS-DA model in between safe and unsafe groups of tomato samples.

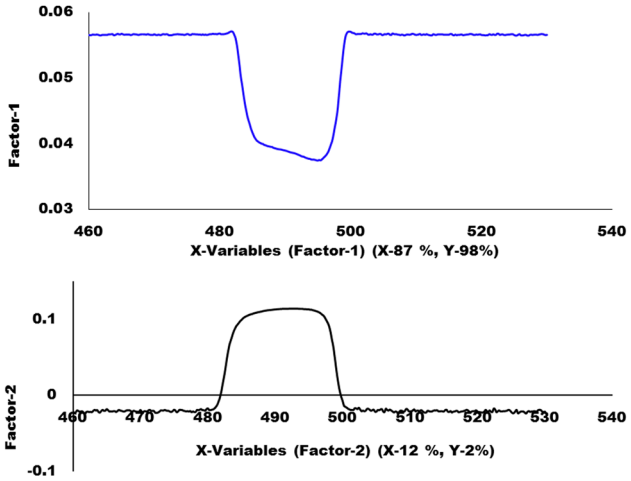

Figure 7: Loading plots of factors 1 and 2 of PLS-DA model.

The score plot of the PLS-DA model as illustrated in Figure 6 represented that factor-1 contributes more to discriminate between two groups as compared to factor-2. It showed a complete discrimination between the samples of the safe group and from unsafe. Factor-1, further showed that 87% of the spectral variation and 98% of the *Y* dummy variability were used during the PLS-DA model. It is a good amount of both *X* and *Y* variables and that plays a very important role in discrimination. The loading plots for both factor 1 and factor 2 of the PLS-DA model are given in Figure 7. The performance of the PLS-DA model was also externally validated by using a test set of samples that were kept aside during the PLS-DA calibration model, as shown in Figure 8.

Figure 8a showed the predicted values of the unidentified samples, while the horizontal lines having estimated uncertainties revealed the vertical lines for the best calibration model, and its limits of detection (LOD's) were calculated based on the standard deviation of the response (Sy) and the slope of the regression curve (*S*) according to the formula: LOD = 3.3(Sy/*S*). From the regression curve, the standard deviation of the response (Sy) value is 0.0628 and the slope of the calibration curve (*S*) value = 0.995, Substituting in the above formula = LOD = 3.3(Sy/*S*) = 3.3* (0.0628/0.9950) = 0.20, While the limit of quantification was calculated as LOQ = 10(Sy/*S*) = 10 × (0.0628/0.9950) = 0.63. As can be seen from Figure 8a and b, all samples of both the safe and unsafe were perfectly predicted by the PLS-DA calibration model and they have values almost close to −1, and +1 which assigns them to class safe and unsafe, respectively.

3.9 Principal component analysis (PCA)

PCA, an unsupervised multivariate exploratory data analysis tool, primarily reveals the hidden structure of large datasets, minimizes multidimensional datasets without loss of information, and provides important information from

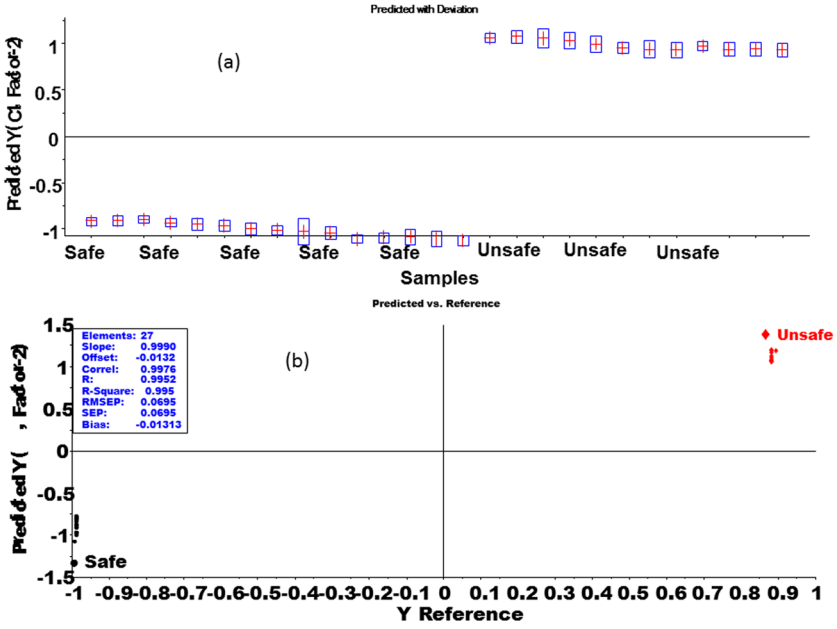

Figure 8: External validation results of PLS-DA model on the test set of both the safe and unsafe groups of tomato samples. (a) prediction vs deviation and (b) prediction vs reference.

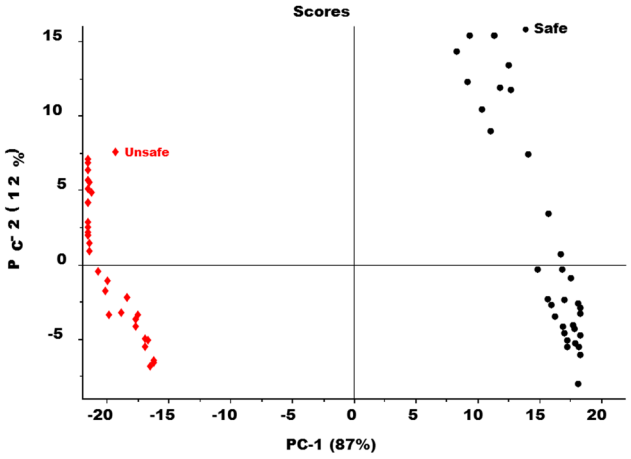

Figure 9: Score plot of PCA model for both safe and unsafe groups of tomato samples.

the data, to recognize noise and outliers in the dataset and to envisage the pattern of grouping based on resemblances and dis-similarities in the data. In the projection method, all the information from the original variable is projected onto a small number of latent variables called principal components (PCs). Each PC summarizes a certain amount of all information comprised in the original data and the first PC covers the maximum source of information in the dataset. PCA analysis transforms a set of related variables into a new set of variables (principal components) that may not be correlated. The PCA transforms the total variance of the dataset so that the first principal component has the largest possible variance, followed by the second largest variance.

In this study, PCA with projection was applied to classify the samples between the two groups of tomato samples defined as safe group (no-spray of insecticide solution) and unsafe group (tomato samples sprayed with abamectin solution).

In order to build the PCA models, the raw emission spectra were split into two sets; i.e., a training test included 70% of all the spectral data to build the PCA calibration model and a test set including 30% of spectral data to externally validate the PCA model. The tested samples from the training set were randomly selected. The PCA calibration models were also internally validated, using a complete cross-validation process using the Singular Value Decomposition (SVD) algorithm with 67 segments and a total of 7 components. The score plot of PCA model for both safe and unsafe groups of tomato samples is shown in Figure 9.

The PCA score plot in Figure 8 determined the complete segregation of the safe group of tomato samples from the unsafe one. However, the separation between the both groups is clearly seen along PC-2. The score plot of the PCA model also determined that PC-1 contributed more to separating between two groups as compared to factor-2. PC-1 carries 87% of the spectral variation and PC2, 12% respectively.

The performance of the PCA calibration model was also externally validated by the projection method using a test set of samples that were kept aside during the PCA calibration model, as shown in Figure 10.

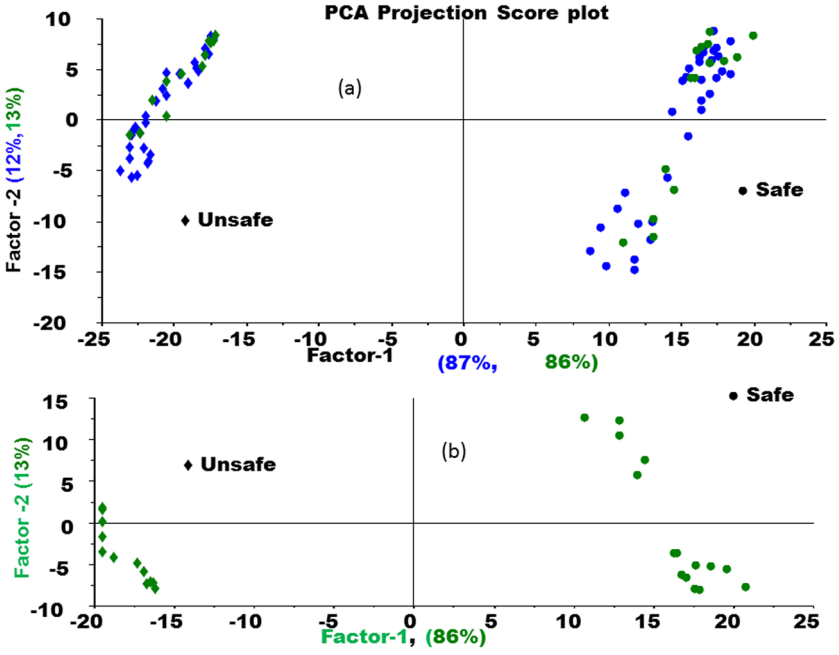

Figure 10: Projection plot for PCA calibration model as an external validation too. (a) PCA projection score plot and (b) PCA score plot.

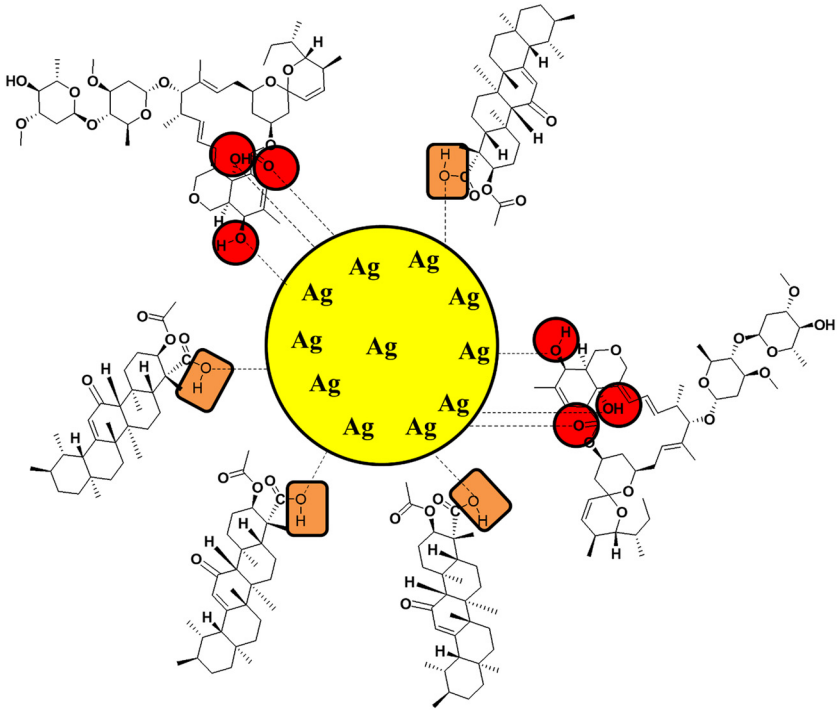

Figure 11: Sensing mechanism showing interaction of abamectin to surface of AKBA-Ag NPs.

Figure 10 shows the PCA projection plot for the PCA calibration model as an external validation result (test set samples). As we can see from Figure 9, the prediction results of the PCA calibration model using the projection method. The green color samples are the results of the projection those illustrate a complete separation and classification of the samples of the safe group of tomato samples from the unsafe one.

3.10 Mechanism of sensing of AKBA-Ag NPs for abamectin

The fluorescence detection can be proceeded by diverse mechanisms, with changes in the fluorescence signal of the system acting as the transducing element [49]. More specifically, changes in the fluorescence signal upon the introduction of pesticides are most often “turn-off” changes,

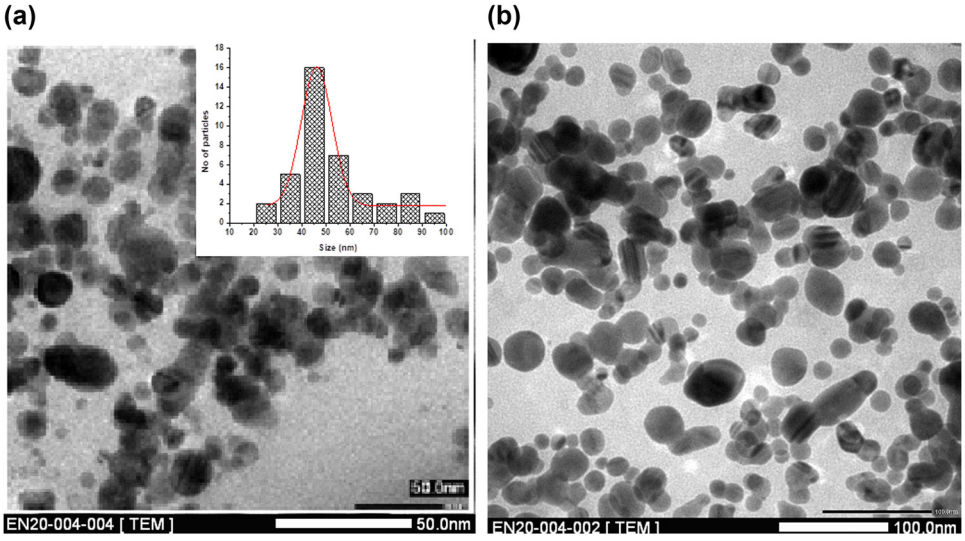

Figure 12: TEM images of AKBA-Ag NPs (a) before and (b) after interaction with abamectin.

resulting from pesticide-induced fluorescence quenching. The fluorescence quenching involves energy transfer of the sensor to the pesticide, which is a result of Forster resonance energy transfer, photoinduced electron transfer, and electron exchange. The mechanism involves Forster resonance energy transfer which has been used extensively. The practical challenges in this mechanism relate to the need for spectral overlap and the fact that there is often undesired overlap between the emission spectra of the donor and the acceptor. The sensitivity of fluorescence-based turn-on sensors may be hampered by this unintended overlap since residual donor emission may still be seen even in the absence of energy transfer [50]. The mechanism is also confirmed through FT-IR analysis (Figure 11).

3.10.1 Morphological changes through TEM analyses

Biosensing capability of AKBA-Ag NPs for abamectin was confirmed from FTIR and fluorescent studies. TEM analyses for both AKBA-Ag NPs and after complexation of AKBA-Ag NPs with abamectin were carried out. TEM images showed a considerable increase in the particles size of AKBA-Ag NPs after interaction with abamectin. The average particle size of AKBA-Ag NPs was a range of 46.2 ± 2 nm to lumps of macro-sized particles. After conjugation with abamectin, the size of the complex (AKBA-Ag NPs and abamectin) was significantly increased, i.e., 64 ± 2.4 but the shape remained the same (Figure 12).

4 Conclusions

Here, we report a simple method for syntheses of AKBA-Ag NPs and their sensing capability against abamectin. AKBA-Ag NPs and abamectin complex and AKBA-Ag nanoparticles were characterized using FTIR, TEM, fluorescence, and UV–Vis spectroscopy. AKBA-Ag NPs and abamectin complex and AKBA-Ag nanoparticles were characterized using FTIR, TEM, fluorescence, and UV–Vis spectroscopy. However, neutral (pH 7) and basic pH (8–12) were found to be suitable for actual protocol, and in conclusion, the AKBA-Ag NPs act as an excellent nanosensor/adsorbent for Abamectin in neutral and basic medium.

Mechanistic study of AKBA-Ag NPs and abamectin was completed via FTIR spectral analyses. FTIR study showed interaction of –OH and –C═O functional moiety of abamectin with silver nano surface. This newly synthesized AKBA-nanoparticle chemosensor can be used as a sensor for the fast detection of abamectin insecticide in tomato paste solutions. PLS-DA models for raw emission spectra were found the optimum ones, based on the lowest values of RMSECV = 0.066 and R^2 = 0.995 for the calibration set, the lowest values of RMSEP = 0.069 and R^2 = 0.995 for the prediction set, and the least number of factors, i.e., 2 and 100% classification among the samples of safe and unsafe tomatoes for both the calibration and prediction sets.

Similarly, the prediction results of the PCA calibration model using the projection method illustrated a complete separation and classification among the samples of a safe group of tomato samples from an unsafe one. The unique sensor (i.e., AKBA-Ag NPs) has a detection limit for abamectin, as low as 0.1 ppm within 20 min response time, which is very advantageous for the fast and sensitive detection of abamectin. Established protocol can also be applicable for the detection of abamectin in environmental and biological samples.

Acknowledgement: The authors are grateful to the University of Nizwa for providing well-established lab facilities. We are also thankful to the analytical and technical staff for their assistance.

Funding information: The project was supported by a grant from The Oman Research Council (TRC) through the funded project (BFP/RGP/HSS/23/037).

Author contributions: AK and AAH conceived and designed the study. TA, FM, and RS performed experiments. NR performed isolation. RC and RB analyzed the data. AK and AAH wrote the manuscript with inputs and comments from all co-authors. All authors have gone through the final version of the manuscript and approved it.

Conflict of interest: The authors state no conflict of interest.

Data availability statement: The datasets generated during and analyzed during the current study are available from the corresponding author on reasonable request.

References

[1] Scognamiglio V, Arduini F, Palleschi G, Rea G. Biosensing technology for sustainable food safety. TrAC Trends Anal Chem. 2014;62:1–10.

[2] Liu S, Zheng Z, Li X. Advances in pesticide biosensors: Current status, challenges, and future perspectives. Anal Bioanal Chem. 2013;405(1):63–90.

[3] Gong J, Wang X, Li X, Wang K. Highly sensitive visible light activated photoelectrochemical biosensing of organophosphate pesticide using biofunctional crossed bismuth oxyiodide flake arrays. Biosens Bioelectron. 2012;38(1):43–9.

[4] Liang M, Fan K, Pan Y, Jiang H, Wang F, Yang D, et al. Fe3O4 magnetic nanoparticle peroxidase mimetic-based colorimetric assay for the rapid detection of organophosphorus pesticide and nerve agent. Anal Chem. 2012;85(1):308–12.
[5] Hu Y, Li X, Zhang L, Zhou M, Wang G, Zhang Y, et al. Mesoporous alumina as a solid phase extraction adsorbent for the determination of abamectin and ivermectin in vegetables by liquid chromatography-tandem mass spectrometry. Anal Methods. 2014;6(13):4734–41.
[6] Zhang K, Yu T, Liu F, Sun M, Yu H, Liu B, et al. Selective fluorescence turn-on and ratiometric detection of organophosphate using dual-emitting Mn-doped ZnS nanocrystal probe. Anal Chem. 2014;86(23):11727–33.
[7] Chauhan N, Pundir CS. An amperometric acetylcholinesterase sensor based on Fe3O4 nanoparticle/multi-walled carbon nanotube-modified ITO-coated glass plate for the detection of pesticides. Electrochim Acta. 2012;67:79–86.
[8] Arduini F, Cinti S, Scognamiglio V, Moscone D. Nanomaterials in electrochemical biosensors for pesticide detection: advances and challenges in food analysis. Microchim Acta. 2016;183(7):2063–83.
[9] Caixach J, Bartolomé A. Analysis of EU legislated compounds for assessing chemical status: main challenges and inconsistencies. In Experiences from surface water quality monitoring. Switzerland: Springer; 2015. p. 269–81.
[10] Campuzano S, Yáez-Sedeño P, Pingarrón JM. Electrochemical affinity biosensors in food safety. Chemosensors. 2017;5(1):8.
[11] Del Carlo M, Compagnone D. Recent strategies for the biological sensing of pesticides: from the design to the application in real samples. Bioanal Rev. 2010;1(2–4):159–76.
[12] Rotariu L, Lagarde F, Jaffrezic-Renault N, Bala C. Electrochemical biosensors for fast detection of food contaminants–trends and perspective. TrAC Trends Anal Chem. 2016;79:80–7.
[13] Kumar V, Arora K. Trends in nano-inspired biosensors for plants. Mater Sci Energy Technol. 2020;3:255–73.
[14] Scognamiglio V. Nanotechnology in glucose monitoring: advances and challenges in the last 10 years. Biosens Bioelectron. 2013;47:12–25.
[15] Shi X, Gu W, Li B, Chen N, Zhao K, Xian Y. Enzymatic biosensors based on the use of metal oxide nanoparticles. Microchim Acta. 2014;181(1–2):1–22.
[16] Viswanathan S, Radecka H, Radecki J. Electrochemical biosensors for food analysis. Monatsh Chem-Chem Monthly. 2009;140(8):891.
[17] Wu J, Zhu Y, Xue F, Mei Z, Yao L, Wang X, et al. Recent trends in SELEX technique and its application to food safety monitoring. Microchim Acta. 2014;181(5–6):479–91.
[18] Zhang L, Wang J, Tian Y. Electrochemical in-vivo sensors using nanomaterials made from carbon species, noble metals, or semiconductors. Microchim Acta. 2014;181(13–14):1471–84.
[19] Campos F, Dybas RA, Krupa DA. Susceptibility of twospotted spider mite (Acari: Tetranychidae) populations in California to Ahamectin. J Econ Entomol. 1995;88(2):225–31.
[20] Putter I, Mac Connell J, Preiser F, Haidri A, Ristich S, Dybas R. Avermectins: novel insecticides, acaricides and nematicides from a soil microorganism. Experientia. 1981;37(9):963–4.
[21] Lasota J, Dybas R. Abamectin as a pesticide for agricultural use. Acta Leidensia. 1990;59(1–2):217–25.
[22] Tišler T, Eržen NK. Abamectin in the aquatic environment. Ecotoxicology. 2006;15(6):495–502.
[23] Suvarna V. Ivermectin: A critical review on characteristics, properties, and analytical methods. J AOAC Int. 2023;106(3):534–57.
[24] Qiao L, Xu J, Yang Z, Li X, Chen L, Sun H, et al. Residual risk of avermectins in food products of animal origin and their research progress on toxicity and determination. Food Rev Int. 2023;39(9):7019–47.
[25] Organization WH. Pesticide Residues in Food, 1997: Report of the Joint Meeting of the FAO Panel of Experts on Pesticide Residues in Food and the Environment and the WHO Core Assessment Group on Pesticide Residues, Lyons, France 22 Sept.-1 Oct. 1997. Vol. 145. Food & Agriculture Org.; 1998.
[26] Lisha KP, Anshup, Pradeep T. Enhanced visual detection of pesticides using gold nanoparticles. J Environ Sci Health Part B. 2009;44(7):697–705.
[27] Jamalipour P, Choobkar N, Abrishamkar M, Pournamdari E. Fluorescent method for determination of residue toxic insecticide abamectin using PbS quantum dots-based gelatin in water samples. Quantum 22:23.
[28] Khalilian F, Rezaee M, Gorgabi MK. Magnetic polypyrrole/Fe_3O_4 particles as an effective sorbent for the extraction of abamectin from fruit juices using magnetic solid-phase extraction combined with dispersive liquid–liquid microextraction. Anal Methods. 2015;7(5):2182–9.
[29] Zhang P, Ding J, Hou J, Zhao L, Chen Y, Ding L. Dynamic microwave assisted extraction coupled with matrix solid phase dispersion for the determination of chlorfenapyr and abamectin in rice by LC-MS/MS. Microchem J. 2017;133:404–11.
[30] Chen M, Ding S, Wen K, Xie S, Wang Q, Pei X, et al. Development of a fluorescence-linked immunosorbent assay for detection of avermectins using a fluorescent single-domain antibody. Anal Methods. 2015;7(9):3728–34.
[31] Cheng C, Liu L-C. On-line solid-phase extraction coupled liquid chromatography-ESI-ion trap-mass spectrometry for analysis of abamectin and ivermectin residues in milk. Anal Methods. 2014;6(5):1581–9.
[32] Farooq S, Chen B, Ahmad S, Muhammad I, Hussain Q, Wu H. Room-temperature, ionic-liquid-enhanced, beta-cyclodextrin-based, molecularly imprinted polymers for the selective extraction of abamectin. Nanomaterials. 2022;12(6):1017.
[33] Guo Z, Su Y, Li K, Tang M, Li Q, Xu S. A highly sensitive octopus-like azobenzene fluorescent probe for determination of abamectin B1 in apples. Sci Rep. 2021;11(1):4655.
[34] Zhao J, Li Z-Y, Zhu J-H, Ji S-L, Liu Y-S, Liu Q-W, et al. Determination of abamectin in food based on magnetic covalent organic frameworks and HPLC-FLD. J Food Compos Anal. 2024;130:106199.
[35] Mertens M, Buettner A, Kirchhoff E. The volatile constituents of frankincense–a review. Flavour Fragr J. 2009;24(6):279–300.
[36] Sharma A, Chhikara S, Ghodekar S, Bhatia S, Kharya M, Gajbhiye V, et al. Phytochemical and Pharmacological investigations on Boswellia serrata. Pharmacogn Rev. 2009;3(5):206.
[37] Ahmed HH, Abd-Rabou AA, Hassan AZ, Kotob SE. Phytochemical analysis and anti-cancer investigation of *Boswellia serrata* bioactive constituents in vitro. Asian Pac J Cancer Prev. 2015;16(16):-7179–88.
[38] Han L, Xia Q, Zhang L, Zhang X, Li X, Zhang S, et al. Induction of developmental toxicity and cardiotoxicity in zebrafish embryos/larvae by acetyl-11-keto-β-boswellic acid (AKBA) through oxidative stress. Drug Chem Toxicol. 2022;45(1):143–50.
[39] Gerbeth K, Hüsch J, Fricker G, Werz O, Schubert-Zsilavecz M, Abdel-Tawab M. In vitro metabolism, permeation, and brain availability of six major boswellic acids from Boswellia serrata gum resins. Fitoterapia. 2013;84:99–106.

[40] Bishnoi M, Patil C, Kumar A, Kulkarni S. Protective effects of nimesulide (COX Inhibitor), AKBA (5-LOX Inhibitor), and their combination in aging-associated abnormalities in mice. Methods Find Exp Clin Pharmacol. 2005;27(7):465–70.
[41] Raja AF, Ali F, Khan IA, Shawl AS, Arora DS. Acetyl-11-keto-β-boswellic acid (AKBA); targeting oral cavity pathogens. BMC Res Notes. 2011;4:1–8.
[42] Caliebe RH, Scior T, Ammon HP. Binding of boswellic acids to functional proteins of the SARS-CoV-2 virus: Bioinformatic studies. Arch Pharm. 2021;354(11):2100160.
[43] Khan A, Al-Harrasi A, Rehman NU, Sarwar R, Ahmad T, Ghaffar R, et al. Loading AKBA on surface of silver nanoparticles to improve their sedative-hypnotic and anti-inflammatory efficacies. Nanomedicine. 2019;14(21):2783–98.
[44] Naresh V, Lee N. A review on biosensors and recent development of nanostructured materials-enabled biosensors. Sensors. 2021;21(4):1109.
[45] Ojea-Jiménez I, Puntes V. Instability of cationic gold nanoparticle bioconjugates: the role of citrate ions. J Am Chem Soc. 2009;131(37):13320–7.
[46] Qiu L, Shao Z, Yang M, Wang W, Wang F, Wan J, et al. Study on effects of carboxymethyl cellulose lithium (CMC-Li) synthesis and electrospinning on high-rate lithium ion batteries. Cellulose. 2014;21(1):615–26.
[47] Gao H, Yang H, Wang C. Controllable preparation and mechanism of nano-silver mediated by the microemulsion system of the clove oil. Results Phys. 2017;7:3130–6.
[48] Siddiqui A, Anwar H, Ahmed SW, Naqvi S, Shah MR, Ahmed A, et al. Synthesis and sensitive detection of doxycycline with sodium bis 2-ethylhexylsulfosuccinate based silver nanoparticle. Spectrochim Acta Part A: Mol Biomol Spectrosc. 2020;225:117489.
[49] Wu L, Huang C, Emery BP, Sedgwick AC, Bull SD, He X-P, et al. Förster resonance energy transfer (FRET)-based small-molecule sensors and imaging agents. Chem Soc Rev. 2020;49(15):-5110–39.
[50] Hsu L-Y, Ding W, Schatz GC. Plasmon-coupled resonance energy transfer. J Phys Chem Lett. 2017;8(10):2357–67.